100. Cyclic Heptapeptides Axinastatin 2, 3, and 4: Conformational Analysis and Evaluation of the Biological Potential

by **Oliver Mechnich**, **Gerhard Hessler**, and **Horst Kessler***

Institut für Organische Chemie und Biochemie, Technische Universität München, Lichtenbergstrasse 4, D-85747 Garching

and **Michael Bernd** and **Bernhard Kutscher**

ASTA Medica AG, Weissmüllerstrasse 45, D-60314 Frankfurt am Main

Dedicated to *Ernst Bayer* on the occasion of his 70th birthday

(24.II.97)

The conformational analysis of naturally occurring cytostatic cyclic heptapeptides axinastatin 2, 3, and 4 was carried out by two-dimensional NMR spectroscopy in combination with distance-geometry (DG) and molecular-dynamics (MD) calculations in explicit solvents. The synthesized secondary metabolites were examined in (D_6)DMSO. Axinastatin 2 was also investigated in CD_3OH. In all structures, Pro^2 is in the $i+1$ position of a βI turn and Pro^6 occupies the $i+2$ position of a βVIa turn about the *cis* amide bond between residue 5 and Pro^6. In all peptides, a bifurcated H-bond occurs between residue 4 CO and the amide protons of residue 1 and 7. For axinastatin 2 and 3, an Asn I_g turn was found about Asn^1 and Pro^2. We compared these structures with conformations of cyclic heptapeptides obtained by X-ray and NMR studies. A β-bulge motif with two β turns and one bifurcated H-bond is found as the dominating backbone conformation of cyclic all-L-heptapeptides. Axinastatin 2, 3, and 4 can be characterized by six *trans* and one *cis* amide bond resulting in a βI/βVI(a)-turn motif, a conformation found for many cyclic heptapeptides. Detailed biological tests of the synthetic compounds in different human cancer cell lines indicates these axinastatins to be inactive or of low activity.

1. Introduction. – Due to improved biological screening methods, the role of marine natural products in drug discovery has been greatly increased in the last few years [1]. Especially in the course of anticancer research, many bioactive compounds with a wide array of diverse and novel chemical structures has been isolated from marine animals and plants. A large number of these natural products is under intensive pharmaceutical investigations, like dolastatin 10 [2], halichondrin B [3], didemnin B [4], and bryostatin 1 [5]. One of these compounds, bryostatin, has recently completed phase-I clinical trials in the USA [6] and is in phase-II trials in Europe [1] as an anticancer agent.

During the last years, many cyclic peptides with cancer cell growth inhibitory properties, such as stylopeptide [7], stylostatin 1 [8], hymenistatin 1 [9], and axinastatin 1 [10], were obtained from marine sources. Cyclic compounds have a restricted conformational space. The determination of their conformation in solution by NMR spectroscopy and MD calculations might result in the design of new lead structures [11].

Three new members of the axinastatin group, the cyclic heptapeptides axinastatin 2 (**1**), 3 (**2**), and 4 (**3**), recently isolated by *Pettit* and coworkers in 10^{-7}–10^{-6}% yield from the marine sponges *Axinella sp.* and *Axinella cf. carteri*, were found to be potent cancer

cell growth inhibitors with GI_{50} values of 0.35 to 0.0072 μg/ml against six human cancer cell lines [12] [13].

To provide sufficient amounts for further structural and pharmaceutical investigations, we have worked out an efficient synthetic route to axinastatin 2 (**1**), 3 (**2**), and 4 (**3**) [14]. By comparing the MS and NMR data of the synthetic compounds with the natural products, we could verify the primary structure of axinastatin 2 (**1**) as cyclo(-Asn^1-Pro^2-Phe^3-Val^4-Leu^5-Pro^6-Val^7-), axinastatin 3 (**2**) as cyclo(-Asn^1-Pro^2-Phe^3-Ile^4-Leu^5-Pro^{6}Val^7-), and axinastatin 4 (**3**) as cyclo(-Thr^1-Pro^2-Leu^3-Trp^4-Val^5-Pro^6-Leu^7-) [14].

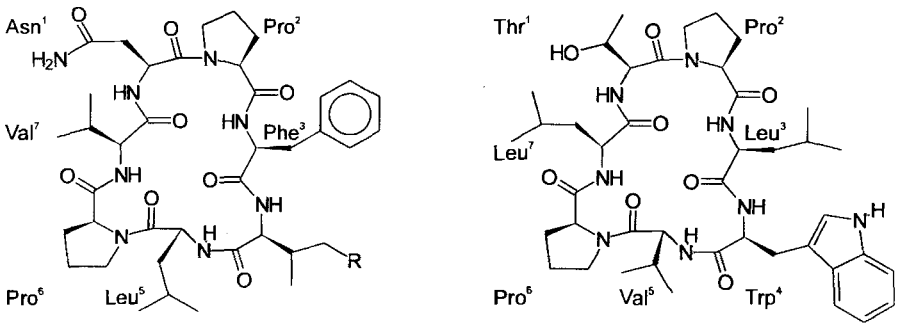

1 R = H axinastatin 2
2 R = Me axinastatin 3

3 axinastatin 4

Fig. 1. *Primary structures of axinastatins 2* (**1**), *3* (**2**), *and 4* (**3**)

Here we present the conformations of axinastatins **2**–**4** (**1**–**3**) in solution, based on homo- and heteronuclear NMR spectroscopy and molecular-dynamics (MD) simulations in explicit solvents. Cyclic peptides have been subjected to many conformational studies, with penta- and hexapeptides receiving the most attention. Cyclic peptides of eight and more residues have also been studied. However, little is known about the conformational behavior of cyclic heptapeptides [15–17].

All three axinastatins were investigated in DMSO which allows a comparison between their conformations. Axinastatin 2 (**1**) was also investigated in MeOH, a solvent with H-bond donating properties, to probe solvent effects on the conformation of these cyclic heptapeptides.

2. Methods. – 2.1. *NMR Studies: Evaluation of Structural Parameters.* The axinastatin 2–4 were investigated in (D_6)DMSO at 300 K, axinastatin 2 (**1**) was also measured in CD_3OH at 300 K. Only one conformer was observed for each of the compounds. ^{1}H- and ^{13}C-NMR chemical shifts were assigned by homo- and heteronuclear 2D techniques [18] [19]. Proton spin systems were unambiguously assigned from TOCSY, P.E.COSY, E.COSY, ROESY, and HMQC-COSY spectra. ^{13}C-Chemical shifts were assigned using HMQC, HMQC-COSY, and HMBC spectra. Sequential assignments of the spin systems were performed by complementary informations from ROESY and HMBC experiments.

Intramolecular proton/proton distances for MD calculations were extracted from ROESY experiments for all compounds. $^3J(NH,H-C(\alpha))$ coupling constants were obtained from well resolved 1D ^{1}H-NMR spectra. $^3J(H-C(\alpha),H-C(\beta))$ coupling constants were extracted from P.E.COSY experiments for the determination of allowed χ_1 angles. Diastereotopic assignment of all geminal protons was achieved using homonuclear coupling constants and interproton distances derived from ROESY spectra as well as heteronuclear coupling informations from HMBC experiments [20].

2.2. *Computer Simulations.* The structures of axinastatins 2–4 were determined by a combined approach of distance-geometry (DG) calculations using ROE distances and ^3J coupling constants subsequent MD refinements in explicit solvents using ROE distance restraints. Afterwards the restraints were removed (free MD) to examine the stability of the rMD conformation. Solvent accessibility of amide protons was characterized by calculating *r*adial *d*istribution *f*unctions (rdfs).

3. Results and Discussion. – 3.1. *Conformational Analysis.* 3.1.1. *Preliminary Remarks.* Some common structural features of axinastatin 2–4 are obvious from the NMR data[1]). All amide bonds are *trans*-configurated apart from a *cis* amide bond between Xaa^5 and Pro^6, as indicated by the large difference Δ of ^{13}C-NMR chemical shifts of Pro^{6}C(β) and Pro^{6}C(γ) [21] [22] ($\Delta[\delta(\text{Pro}^6\text{C}(\beta))-\delta(\text{Pro}^6\text{C}(\gamma))]$: 30.46–21.27 = 9.19 ppm (**1** in (D$_6$)DMSO); 32.06–22.49 = 9.57 ppm (**1** in CD$_3$OH); 31.35–21.46 = 9.89 ppm (**2** in (D$_6$)DMSO); 29.97–21.48 = 8.49 ppm (**3** in (D$_6$)DMSO)) and the strong $H-C(\alpha)/H-C(\alpha)$ ROEs between these residues.

For all compounds investigated here, temperature gradients of the amide protons (*Table 1*), $^3J(NH,H-C(\alpha))$ coupling constants (*Table 2*), proton/proton distances and even ^{1}H- and ^{13}C-chemical shifts[1]) indicate similar conformational behavior, hence, a detailed discussion is exemplary given for axinastatin 2 (**1**).

Table 1. *Comparison of Temperature Gradients of Amide Protons of Axinastatin 2* (**1**) *in (D$_6$)DMSO and CD$_3$OH and Axinastatin 3* (**2**) *and Axinastatin 4* (**3**) *in (D$_6$)DMSO*

Residue	$-\Delta\delta/\Delta T$ [ppb/K]			
	1 in MeOH	**1** in DMSO	**2** in DMSO	**3** in DMSO
Xaa^{1}NH	0.9	−0.1	−0.3	0.2
Xaa^{3}NH	5.0	2.5	3.3	2.4
Xaa^{4}NH	0.7	−0.5	−0.3	1.4
Xaa^{5}NH	12.2	6.0	6.7	6.9
Xaa^{7}NH	2.8	2.4	1.9	3.6

3.1.2. *Axinastatin 2* (**1**) *in (D$_6$)DMSO and CD$_3$OH. Overall Conformation.* Axinastatin 2 (**1**) has the same overall conformation in (D$_6$)DMSO and CD$_3$OH, as shown by comparison of the NMR data (coupling constants *J*, ROE distances, and temperature coefficients) and structure calculation. The resulting structure of **1** in DMSO averaged

[1]) ^{1}H- and ^{13}C-NMR chemical shifts of axinastatin 3 (**2**) and 4 (**3**) in (D$_6$)DMSO and of axinastatin 2 (**1**) in (D$_6$)DMSO and CD$_3$OH are available on request.

Table 2. *^{3}J(NH,H–C(α)) and ^{3}J(H–C(α), H–C(β)) Coupling Constants* [Hz] *of Axinastatin 2* (**1**) *in (D_6)DMSO and CD_3OH and of Axinastatin 3* (**2**) *and Axinastatin 4* (**3**) *in (D_6)DMSO* (300 K, 500 MHz)

	Xaa^1	Xaa^2	Xaa^3	Xaa^4	Xaa^5	Xaa^6	Xaa^7
^3J(N*H*,H–C(α))							
1 in DMSO	6.1	–	9.6	8.6	5.2	–	8.5
1 in MeOH	5.7	–	9.4	8.9	4.8	–	7.5
2 in DMSO	6.1	–	9.6	8.0	5.4	–	8.2
3 in DMSO	8.0	–	9.4	7.2	4.1	–	8.2
^3J(*H*–C(α)/$H_{pro\text{-}R}$–C(β))							
1 in DMSO	–	9.7	12.0	8.6	12.2	1.0	7.9
1 in MeOH	–	10.4	12.2	9.23	12.3	1.0	7.8
2 in DMSO	–	9.9	9.9	8.2	12.5	1.0	7.9
3 in DMSO	3.2	10.3	–	3.3	5.0	1.0	3.5
^3J(*H*–C(α)/$H_{pro\text{-}S}$(β))							
1 in DMSO	–	7.7	4.2	–	2.2	7.7	–
1 in MeOH	–	8.0	4.4	–	2.6	8.1	–
2 in DMSO	–	7.9	4.3	–	2.5	7.8	–
3 in DMSO	–	8.5	–	10.3	–	8.5	10.0

over the last 50 ps of the 150-ps rMD calculation is shown in *Fig. 2*. The simulation is in reasonable agreement with the experimental data. Calculated and experimental distances listed in *Table 3* are comparable. During 150-ps free MD trajectory following the rMD simulation, the described conformation remains stable (*Table 3*) and, therefore, proved to be energetically favorable.

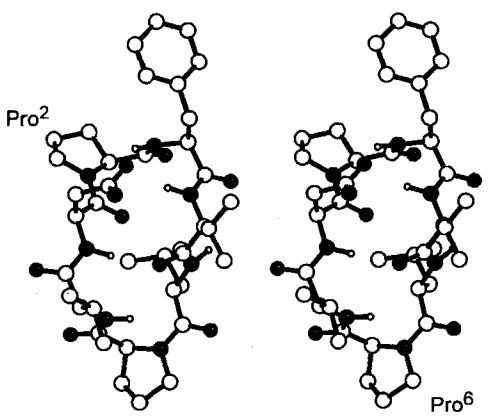

Fig. 2. *Conformation of axinastatin 2* (**1**) *in DMSO obtained by averaging over the last 50 ps of the rMD trajectory and subsequent energy-minimization for 300 steps steepest descent*

Backbone Conformation. Axinastatin 2 (**1**) is characterized by a βI turn with Pro^2 in the $i + 1$ position and a βVI(a) turn with Leu^5 in the $i + 1$ position. A bifurcated H-bond is observed between Val^{7}N*H*, Asn^{1}N*H*, and Val^{4}CO. This H-bonding pattern is confirmed by the low solvent accessibility of the Val^{7}N*H* and Asn^{1}N*H*, wich is indicated by

Table 3. *Proton-Proton Distances Derived from a ROESY Experiment at 300 K for Axinastatin 2* (**1**) *in* (D_6)*DMSO in Comparison with Distances Obtained from MD Calculations.* Experimental distances are calibrated on the average distance between the geminal $H-C(\beta)$ protons of Pro^2, Leu^5, and Pro^6 (178 pm). Deviations of calculated distances larger than 30 pm of upper and lower limit (10%) are given in *italics*.

Proton-proton distances	d_{exp} [pm]	d_{rMD} [pm]	d_{fMD} [pm]
Leu^5NH/Val^4NH	381	378	387
Phe^3NH/Val^4NH	215	247	249
$Asn^1NH/Leu^5H-C(\alpha)$	258[a])	304	*325*
$Phe^3NH/Asn^1H-C(\alpha)$	407	455	460
$Phe^3NH/Pro^2H-C(\alpha)$	314	345	345
$Leu^5NH/Val^4H-C(\alpha)$	200	224	223
$Val^7NH/Pro^6H-C(\alpha)$	299[a])	324	307
$Val^7NH/Leu^5H-C(\alpha)$	239[a])	257	240
$Asn^1NH/Val^7H-C(\alpha)$	317[a])	358	358
$Val^4NH/Phe^3H-C(\alpha)$	299	357	358
$Asn^1NH/Val^4H-C(\beta)$	370[a])	400	379
$Asn^1NH/ValH-C(\beta)$	267[a])	262	253
$Asn^1H-C(\alpha)/Pro^2H_{pro\text{-}R}-C(\delta)$	206	229	233
$Pro^2H_{pro\text{-}R}-C(\delta)/Asn^1H_{pro\text{-}R/pro\text{-}S}-C(\beta)$	281	336[b])	347[b])
$Pro^2H_{pro\text{-}S}-C(\delta)/Asn^1H_{pro\text{-}R/pro\text{-}S}-C(\beta)$	228	316[b])	312[b])
$Phe^3NH/Pro^2H_{pro\text{-}S}-C(\delta)$	297	316	332
$Phe^3NH/Pro^2H_{pro\text{-}R}-C(\beta)$	302	307	303
$Phe^3H-C(2, 6)/Pro^2H_{pro\text{-}S}-C(\delta)$	337	552[b])	600[b])
$Phe^3H-C(3, 5)/Pro^2H_{pro\text{-}S}-C(\delta)$	368	*642*[b])	*720*[b])
$Pro^6H-C(\alpha)/Leu^5H-C(\alpha)$	211	242	233
$Pro^6H-C(\alpha)/Leu^5H_{pro\text{-}S}-C(\beta)$	221	247	256
$Val^7NH/Pro^6H_{pro\text{-}S}-C(\delta)$	299[a])	331	346
$Val^7NH/Pro^6H_{pro\text{-}R}-C(\beta)$	437[a])	420	427
$Val^7NH/pro^6H_{pro\text{-}S}-C(\gamma)$	331[a])	358	375
$Asn^1NH/H-C(\alpha)$	263	302	303
$Asn^1NH/H_{pro\text{-}R/pro\text{-}S}-C(\beta)$	284	303[b])	298[b])
$Pro^2H-C(\alpha)/H_{pro\text{-}S}-C(\beta)$	220	237	238
$Pro^2H-C(\alpha)H_{pro\text{-}R}-C(\beta)$	299	305	304
$Pro^2H-C(\alpha)H_{pro\text{-}R/pro\text{-}S}-C(\gamma)$	262	290[b])	290[b])
$Pro^2H_{pro\text{-}S}-C(\delta)/H_{pro\text{-}R}-C(\beta)$	273	286	295
$Pro^2H_{pro\text{-}R}-C(\delta)/H_{pro\text{-}S}-C(\beta)$	373	419	402
$Phe^3NH/H-C(\alpha)$	268[a])	304	304
$Phe^3NH/H_{pro\text{-}S}-C(\beta)$	312[a])	377	373
$Phe^3NH/H_{pro\text{-}R}-C(\beta)$	238[a])	262	255
$Phe^3H-C(\alpha)/H_{pro\text{-}R}-C(\beta)$	306	307	307
$Phe^3H-C(\alpha)/H_{pro\text{-}S}-C(\beta)$	242	252	258
$Val^4NH/H-C(\alpha)$	265	306	306
$Val^4NH/H-C(\beta)$	259	279	273
$Val^4H-C(\alpha)/H-C(\beta)$	244	*305*	*306*
$Leu^5NH/H-C(\alpha)$	260	292	294
$Leu^5NH/H-C(\gamma)$	231	264	257
$Leu^5NH/H_{pro\text{-}R}-C(\beta)$	226	244	246
$Leu^5H-C(\alpha)/H-C(\gamma)$	280	283	298
$Leu^5H-C(\alpha)/H_{pro\text{-}R}-C(\beta)$	309	309	306
$Leu^5H-C(\alpha)/H_{pro\text{-}S}-C(\beta)$	246	261	259
$Pro^6H-C(\alpha)/H_{pro\text{-}R}-C(\delta)$	356	380	385
$Pro^6H-C(\alpha)/H_{pro\text{-}S}-C(\delta)$	400	417	416
$Pro^6H-C(\alpha)/H_{pro\text{-}R}-C(\beta)$	259	272	271

Table 3 (cont.)

Proton-proton distances	d_{exp} [pm]	d_{rMD} [pm]	d_{fMD} [pm]
Pro^6*H*–C(α)/$H_{pro\text{-}S}$–C(β)	225	231	232
Pro^6*H*–C(α)/$H_{pro\text{-}R}$–C(γ)	329	*415*	*415*
Pro$^6H_{pro\text{-}R}$–C(δ)/$H_{pro\text{-}S}$–C(β)	289	300	304
Pro$^6H_{pro\text{-}R}$–C(δ)/$H_{pro\text{-}R}$–C(γ)	237	238	237
Pro$^6H_{pro\text{-}S}$–C(δ)/$H_{pro\text{-}S}$–C(β)	452	389	389
Pro$^6H_{pro\text{-}S}$–C(δ)/$H_{pro\text{-}R}$–C(γ)	329	280	281
Pro$^6H_{pro\text{-}S}$–C(δ)/$H_{pro\text{-}S}$–C(γ)	237	236	236
Pro$^6H_{pro\text{-}R}$–C(β)/$H_{pro\text{-}R}$–C(γ)	237	269	270
Pro$^6H_{pro\text{-}R}$–C(β)/$H_{pro\text{-}S}$–C(γ)	247	244	244
Val^{7}N*H*/*H*–C(α)	278[a])	298	300
Val^{7}N*H*/*H*–C(β)	249[a])	258	261
Val^7*H*–C(α)/*H*–C(β)	242	*306*	*305*

[a]) Distances were obtained from ROESY experiments at 294 K.

[b]) Distances are given to the corresponding C-atom. For those distance restraints, a pseudoatom correction was used during the calculation.

their small temperature gradients (*Table 4*). Accordingly, the radial distribution functions (*Fig. 3*) calculated for Val^{7}N*H* and Asn^{1}N*H* from the free MD calculations show solvent shielding.

Table 4. *Population of Significant Hydrogen Bonds Observed during Various Trajectories for Axinastatin 2* (**1**) *in* (D_6)*DMSO Compared with Temperature Gradients of the Amide Protons*

Donor	Acceptor	rMD	fMD	$-\Delta\delta/\Delta T$ [ppb/K]
		Population [%]	Population [%]	
Asn^{1}N*H*	Val^{4}CO	98.5	96.8	−0.1
Phe^{3}N*H*	Asn^{1}CO(γ)	86.3	85.1	2.5
Val^{4}N*H*	Asn^{1}CO	21.1	19.3	−0.5
Val^{4}N*H*	Asn^{1}CO(γ)	83.3	86.1	−0.5
Leu^{5}N*H*	Phe^{3}CO	17.0	31.1	6.0
Val^{7}N*H*	Val^{4}CO	45.0	61.9	2.4

In agreement with the small temperature gradient (2.5 ppb/K), the rdf calculated for Phe^3 (*Fig. 3*) indicates solvent shielding, caused by interaction of the Asn^1 side chain with the peptide backbone by H-bonding between Asn^{1}CO(γ) and Phe^{3}N*H* forming an Asn I_g turn [23]. The Asn turn is topologically similar to a β turn, but the accepting carbonyl O-atom belongs to a side chain and not to the backbone. The four possible Asn turns (I_g, I_t, II_g, II_t) are characterized by the orientation of the Asn^1 side chain ($\chi_1 = 60°$ (g = gauche) or 180° (t = *trans*) and the orientation of the Asn^1-Pro^2 amide plane. The backbone and side-chain dihedral angles of Asn^1 and Pro^2 (ψ(Asn^1) = 169.7°, χ_1(Asn^1) = 70.4°, ϕ(Pro^2) = − 53.6° and ψ(*H*–C) = − 29.9°) are typical for the Asn I_g turn.

The radial distribution function for Val^{4}NH (*Fig. 3*) shows solvent shielding in agreement with the small temperature gradient (−0.5 ppb/K). An additional H-bond between Asn^{1}CO(γ) and Val^{4}N*H* directs the Val^4 amide proton towards the Asn^1 side

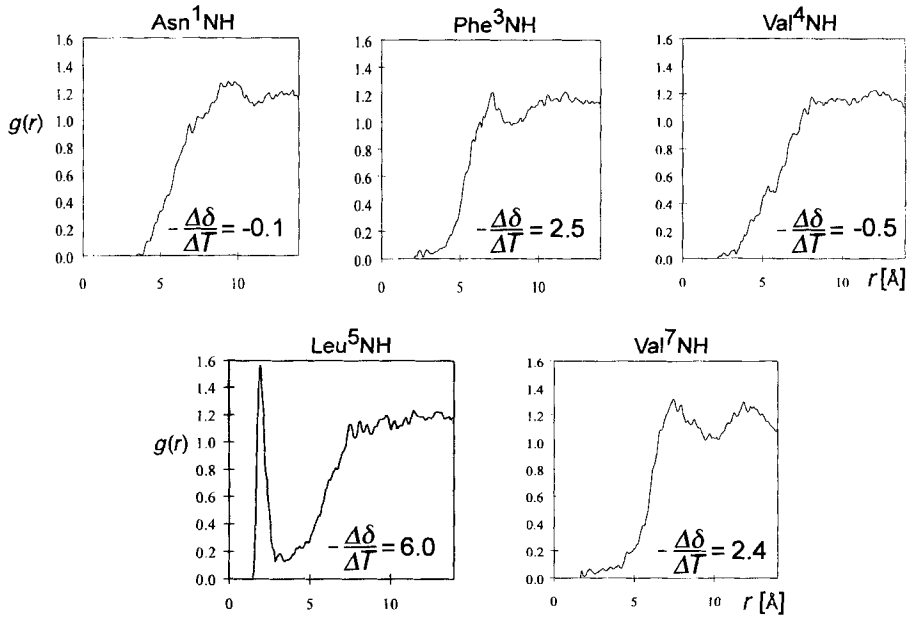

Fig. 3. *Radial distribution functions* (rdf) *obtained from free MD trajectory compared with the temperature gradients* [ppb/K] *of the amide protons of axinastatin 2* (**1**) *in DMSO*

chain and results in a distorted $\psi(i+2)$ angle ($\psi(\text{Phe}^3) = -54°$) compared to an ideal βI turn (*Table 5*). This ψ angle is close to the $\psi(i+2)$ angle of an ideal βIII turn.

Table 5. *Comparison of Backbone and Side-Chain Dihedral Angles* [°] *of the Averaged Conformations of Axinastatin 2* (**1**) *in DMSO and MeOH and of Axinastatin 3* (**2**) *and Axinastatin 4* (**3**) *in DMSO*. The averaged structures were obtained from the last 50 ps of the respective trajectories and subsequent energy-minimization for 300 steps steepest descent.

	Xaa[1]	Xaa[2]	Xaa[3]	Xaa[4]	Xaa[5]	Xaa[6]	Xaa[7]
ϕ[°]							
1 in DMSO	−128.1	−53.6	−80.7	−109.2	−79.4	−85.6	−79.3
1 in MeOH	−137.7	−50.8	−77.2	−112.4	−79.1	−82.1	−70.3
2 in DMSO	−141.6	−53.8	−73.9	−131.6	−81.7	−86.6	−72.5
3 in DMSO	−113.3	−48.5	−68.9	−127.3	−84.8	−101.6	−120.8
ψ[°]							
1 in DMSO	169.7	−29.9	−53.8	90.6	145.1	8.8	−56.7
1 in MeOH	165.5	−32.1	−50.9	90.1	145.9	−9.4	−41.7
2 in DMSO	170.8	−27.9	−44.9	101.1	145.0	4.8	−54.7
3 in DMSO	163.6	−33.7	−43.0	94.2	134.8	58.9	−65.8
χ_1[°]							
1 in DMSO	70.4	−25.1	−61.8	−178.9	−71.8	34.5	178.6
1 in MeOH	73.3	−24.7	−72.3	−179.9	−72.6	30.2	70.1
2 in DMSO	70.9	−25.4	−62.7	−168.6	−69.9	35.5	178.2
3 in DMSO	60.5	−25.3	−172.6	−166.3	172.6	39.4	−176.8

Leu^{5}N*H* is the only amide proton orientated towards the solvent, as shown by the radial distribution function (*Fig. 3*). The function has a pronounced peak indicating the proximity of solvent molecules during the calculation. This is consistent with the observed high temperature gradient of Leu^{5}N*H* (6.0 ppb/K).

The ^3J(N*H*,*H*–C(α)) coupling constants listed in *Table 6* agree reasonably well with the experimental data, considering that the slope of the *Karplus* equation is very steep for this range of ϕ angles. This results in large deviations for the coupling constant in response to only a few degree of deviation of the ϕ angles (10–15°). For Asn^1, the ϕ angles −160° and −80° correspond to the experimental ^3J(N*H*,*H*–C(α)) coupling constant of 6.1 Hz. During the simulation, the ϕ angle of Asn^1 fluctuates between this values resulting in an averaged coupling constant of 9.7 Hz.

Table 6. *Agreement between Calculated and Experimental* ^3J*(NH,H–C(α)) Coupling Constants* [Hz] *for Axinastatin 2* (**1**) *in (D$_6$)DMSO*

	rMD	fMD	Experimental
Asn^{1}N*H*	9.9	10.1	6.1
Phe^{3}N*H*	7.3	7.3	9.6
Val^{4}N*H*	10.1	9.6	8.6
Leu^{5}N*H*	6.7	7.1	5.2
Val^{7}N*H*	6.4	7.6	8.5

Side-Chain Conformation. For Asn^1, the *H*–C(β) protons are degenerated. Therefore, only the sum of the ^3J(*H*–C(α),*H*–C(β)) coupling constants can be determined. The value of *ca.* 10 Hz suggests significant population of a χ_1 angle of 60° (*ca.* 60%) which orientates the side chain over the peptide backbone and allows interaction of Asn^{1}CO(γ) with the amide protons of the backbone resulting in the Asn I_g turn motif. The population of other side-chain rotamers cannot be determined experimentally.

According to a *Pachler* analysis [24], Phe^3 predominantly populates a χ_1 angle of −60° (85%). In agreement with the experimental data, this side-chain conformation allows the formation of a hydrophobic cluster between the side chains of Phe^3 and Pro^2. Hydrophobic clustering is also indicated by a high-field shift of Pro$^2H_{pro\text{-}R}$–C(β) by *ca.* 1 ppm compared to Pro$^2H_{pro\text{-}S}$–C(β), and several ROE cross-peaks between the aromatic side chain of Phe^3 and Pro^2*H*–C(δ).

For Pro^2, a *γ-exo* conformation is found in agreement with ^3J(*H*–C(α),*H*–C(β)) coupling constants and different ROEs between Pro^2*H*–C(α), *H*–C(β), *H*–C(γ), and *H*–C(δ), (*Table 3*).

The Leu^5 side chain adopts a $\chi_1 = -60°$ conformation which is populated to 85% as calculated by *Pachler* analysis. This conformation is confirmed by ROEs and hetero- and homonuclear couplings (^3J(*H*–C(α),$H_{pro\text{-}R}$–C(β)) = 12.2 Hz, ^3J(*H*–C(α), $H_{pro\text{-}S}$–C(β)) = 2.2 Hz).

Pro^6 is involved in a *cis* amide bond and adopts a different conformation than Pro^2. According to the experimental data, Pro^6 forms a *γ-endo* envelope. This conformation which is indicated by the small ^3J(*H*–C(α),$H_{pro\text{-}R}$–C(β)) (1 Hz) seems to be characteristic for *cis*-proline (see *Table 2*, [25] [26]).

For Val^7, the ^3J(*H*–C(α),*H*–C(β)) of *ca.* 7 Hz clearly suggests an equilibrium of several side-chain conformers. Since during the simulation only one rotamer occurs, the

$H-C(\alpha)/H-C(\beta)$ distance restraint is violated. For Val[4], the somewhat larger $^3J(H-C(\alpha), H-C(\beta))$ of 8.6 Hz suggests a greater population of the *anti*-periplanar orientation of the $H-C(\alpha/H-C(\beta)$ protons, but the fairly short $H-C(\alpha)/H-C(\beta)$ distance clearly favors a synclinal orientation. Therefore, the χ_1 angle of Val[4] has to be considered as flexible too.

For axinastatin 2 (**1**) in MeOH, the DG and rMD calculations in explicit MeOH result in a conformation very similar to the one found in DMSO. A superposition of the two structures is shown in *Fig. 4*. The comparison of the NMR data for both solvents gives further evidence that the conformational behavior in both solvents is very similar. Interestingly, for stylostatin 1 (cyclo(-Asn[1]-Ser[2]-Leu[3]-Ala[4]-Ile[5]-Pro[6]-Phe[7])), a cytotoxic cyclic peptide from *Stylotella aurantium* [27], different conformational behavior was found in MeOH and DMSO [28]. The overall shape of the backbone conformations of stylostatin 1 in these solvents are very similar to those of axinastatin 2. Nevertheless, in DMSO, the amide plane between Asn[1] and Ser[2] shows a flip resulting in a transition from an Asn I_g turn to an Asn II_g turn. In methanol the Asn I_g turn remains stabile. Since in the case of axinastatin 2 (**1**) Pro[2] restricts the ϕ angle to a small range around $-60°$, such a transition cannot occur for this compound. These results indicate that the two proline residues in position 2 and 6 induce a fairly rigid backbone conformation of **1**.

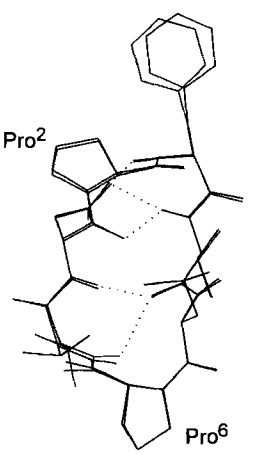

Fig. 4. *Superposition of structures of axinastatin 2* (**1**) *in DMSO and MeOH obtained by averaging over the last 50 ps of the rMD trajectory*. In agreement with the experimental data, similar conformations were found in both solvents.

3.1.3. *Axinastatin 3* (**2**) *in DMSO*. In axinastatin 3 (**2**), Val[4] is replaced by Ile[4] compared to axinastatin 2 (**1**). Since Ile and Val have comparable steric requirements, a similar conformation is expected for **2**. The comparison of chemical shifts, coupling constants, temperature coefficients, ROEs, as well as the result of the structure calculation confirm that expectation. The structure averaged over the last 50 ps of the rMD calculation is almost identical to that one obtained for **1** in DMSO (see superposition in *Fig. 5*).

3.1.4. *Axinastatin 4* (**3**) *in DMSO*. Axinastatin 4 (**3**) has only two residues in common with axinastatin 2 (**1**) and 3 (**2**), namely Pro[2] and Pro[6], while the remaining residues

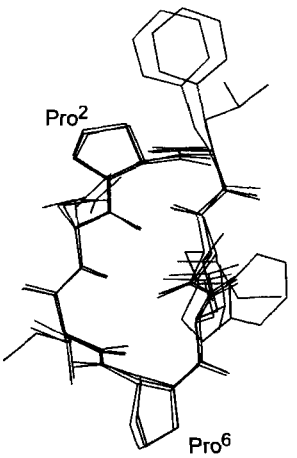

Fig. 5. *Superposition of axinastatin 2,* (**1**), *3* (**2**), *and 4* (**3**) *in DMSO.* The observed similar conformations are in agreement with the experimental data.

differ. Nevertheless, the structures are very similar. The conformation shown in *Fig. 6* was obtained from 150-ps rMD by averaging over the last 50 ps.

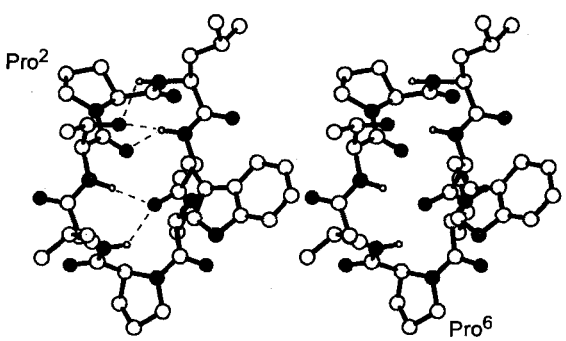

Fig. 6. *Conformation of axinastatin 4* (**3**) *in DMSO obtained by averaging over the last 50 ps of the rMD trajectory and subsequent energy-minimization for 300 steps steepest descent.* According to *Pachler* analysis, side chains of Trp^4 and Leu^7 are found with a χ_1 angle of 180°. Due to contracting NOE and ^3J coupling data, the side chain of Leu^3 is experimentally underdetermined.

The backbone conformation of **3** is similar to that of **1** and **2**. Asn^1 is replaced by Thr^1 which side chain also interacts with the peptide backbone. The additional H-bonds between Thr^1-O(γ) and the amide protons of residue 3 (Leu) and 4 (Trp) stabilize the βI turn. It could be shown, that Ser [29] or Thr [30] in the *i* position of a four-membered turn always induce a βI turn in cyclic peptides, whereas a non-acceptor side chain in position *i* leads to a βI/βII equilibrium.

The side-chain conformations of Pro^2 and Pro^6 of **3** are similar as found for **1** and **2**. According to a *Pachler* analysis, the side chains of Trp^4 and Leu^7 are predominately found with a χ^1 angle of 180° (70%). In agreement with ROEs and coupling constants, Val^5 prefers a *syn*-clinal orientation of the $H-C(\alpha)/H-C(\beta)$ protons.

3.2. *Structural Discussion.* Most known conformations of cyclic all-L-heptapeptides can be systematically classified by their secondary-structure features. For only a few examples such as the X-ray structure of cycloheptasarcosyl [31], no characteristic secondary-structure features were found.

A rare conformational class which is found for the synthetic compound cyclo(-Gly^1-Phe^2-Leu^3-Ala^4-Lys^5(Z)-Tyr^6(Bzl)-Gly^7-) is characterized by a β/γ-turn motif with the β turn about Gly^1 and Phe^2 and a β-sheet-like structure with the γ turn about Lys^5(Z) [17].

In most known structures of cyclic all-L-heptapeptides obtained from X-ray or NMR studies, two β turns and a bifurcated H-bond is the dominating motif of the backbone conformation. Based on the configuration of the amide bond between the $i + 1$ and $i + 2$ position of the two β turns, three general conformation classes (*cis/cis*, *trans/trans*, and *cis/trans*) are possible. To our knowledge, phakellistatin 1 (cyclo(-Pro^1-Ile^2-Pro^3-Ile^4-Phe^5-Pro^6-Tyr^7)) [32] is the only known structure with two *cis* amide bonds in the β turns about Ile^2/Pro^3 and Phe^5/Pro^6. There have been few examples for *trans/trans* configuration in the β turns: pseudostellarin D (cyclo(-Gly^1-Tyr^2-Gly^3-Pro^4-Leu^5-Ile^6-Leu^7)) [16] shows a βII turn about Leu^7 and Gly^1 and a βI turn about Pro^4 and Leu^5, whereas yunnanin A (cyclo(-Gly^1-Tyr^2-Gly^3-Gly^4-Pro^5-Phe^6-Pro^7)) [33] has a βII turn about Pro^7 and Gly^1 and a βII' turn about Gly^4 and Pro^5. The synthetic compound cyclo-(-Ala^1-Ile^2-Val^3-Ser^4(Bzl)-Aib^5-Phe^6-Gly^7-) [17] with *trans*-configurated amide bonds is characterized by β turns about Ala^1/Ile^2 and Aib^5/Phe^6. Most known structures of cyclic all-L-heptapeptides belong to the family with one *cis* and one *trans* amide bond in the β turns. All these peptides, such as evolidine [15] [34], hymenamide B-F [35], stylopeptide [7], isophakellistatin 3 [36], stylostatin 1 [8] [28], and axinastatin 1 [25], form the *cis* amide bond at a proline residue. For all these cyclic heptapeptides, the overall backbone conformation is similar to the structures of axinastatins 2–4, investigated here. The conformational similarity of axinastatins 2–4 is demonstrated by superposition in *Fig. 5* (see above) and by comparison of the dihedral angles (*Table 5*).

In axinastatins 2–4 (**1**–**3**), Pro^2 is in the $i + 1$ position of a βI turn and Pro^6 occupies the $i + 2$ position of a βVI(a) turn about the *cis* amide bond between residue 5 and Pro^6. In all peptides, a bifurcated H-bond occurs between residue-4 CO and the amide protons of residue 1 and 7. Cyclic hexapeptides show a β-sheet-like symmetric H-bond pattern. Due to the asymmetric addition of one residue in heptapeptides, the secondary structure results in an asymmetric arrangement of the β turns. This secondary-structure feature resembles a β-bulge motif. The β-bulge motif [37], which was also described for evolidine [15], often occurs as non-repetitive secondary-structure feature in proteins within antiparallel sheets and is characterized by a bifurcated H-bond between two adjacent amide protons on one strand to one carbonyl O-atom on the other strand. This feature, where the side chains of all three residues are on the same side, results in a bending of the β sheet and is similar to the H-bond pattern found in **1**–**3**.

From the similar conformation of axinastatin 2 (**1**) in solvents of such different properties as DMSO and MeOH, we conclude a preferred backbone conformation. This conformation seems to be induced by the two proline residues in position 2 and 6. Several cyclic heptapeptides isolated from marine sources, such as axinastatin 1 and hymenamide C-E, contain this Pro$^{(6)}$-Xaa-Xaa-Pro$^{(2)}$ segment [35]. All of them have similar conformations confirming the general observation that *trans*-Pro is mainly found in the $i + 1$ position, whereas *cis*-Pro is only found in the $i + 2$ position of a βVIa turn [38]. However,

similar backbone conformations are also found for *cis*-proline-containing structures without the Pro$^{(6)}$-Xaa-Xaa-Pro$^{(2)}$ motif, such as evolidine, hymenamide B and F, stylopeptide, and stylostatin 1. We, therefore, conclude that the conformations of cyclic all-L-heptapeptides are mainly induced by the *cis*-Pro residue in the βVI(a) turn.

This conclusion is confirmed by a comparison of the structures in all three conformational families with the β/β-turn motif. In phakellistatin 1, the two *cis*-Pro residues occupy the $i + 2$ positions of the β turn. As mentioned above, the synthetic compound cyclo(-Ala^1-Ile^2-Val^3-Ser^4(Bzl)-Xaa^5-Phe^6-Gly^7-) for Xaa^5 = Aib^5 exists in all-*trans* configuration. The replacement of Aib^5 by Pro^5 results in a formation of a *cis* amide bond between Ser^4(Bzl) and Pro^5 shifting the β turn from Aib^5/Phe^6 to Ser^4(Bzl)/Pro^5 [17].

More generally, conformations of small cyclic peptides can be rationalized by a comparison with the conformation of cycloalkenes and cycloalkanes [39]. As depicted in *Fig. 7*, the peptide bond is equivalent to a C=C bond (*E* or *Z*) yielding an olefin. According to *Dunitz* and *Waser* [40], the conformational behavior of cycloalkenes can be further reduced by substitution of an (*E*) double bond by a single bond and of a (*Z*) double bond by a pseudo-CH_2 group.

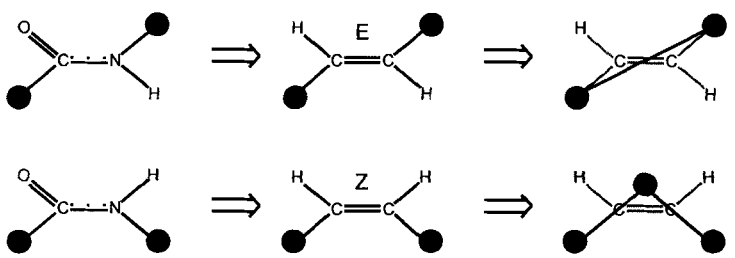

Fig. 7. *Schematic description of the extension of the* Dunitz-Waser *concept to peptides*

Fig. 8, a shows the side view of the overall shape of the bent backbone of axinastatin 2 (**1**) in DMSO. As depicted in *Fig. 8, b*, and *8, c*, each *trans* peptide bond of **1** is reduced to a single bond connecting the two adjacent C(α) atoms, whereas the *cis* amide bond is substituted by a pseudo-CH_2 group. As we found already for cyclic tetra-, penta-, and hexapeptides, the resulting conformation is surprisingly similar to the most stable conformation of the corresponding cycloalkane [39]. In the case of the cyclic heptapeptides described here, the conformation matches the shape of the cyclooctane, which is mainly found in a boat-chair conformation [41] [42]. Exemplary, the crystal structure of *cis*-cyclooctane-1,5-diol [42] is depicted in *Fig. 9, a*. Similar to it, axinastatin 2 (**1**) shows an overall boat-chair backbone conformation (*Fig. 9, b*).

On the first glance, the overall similarity of cyclic-peptide conformations and cycloalkanes is surprising. The distance from side chain to side chain in the reduced cyclic peptide is larger than 3.5 Å. Therefore, a direct interaction of the side chains as in cycloalkanes cannot be expected. We, therefore, assume that the 'steric effects' between C(α) atoms are transmitted *via* the connecting amide bond. This can be rationalized by the prefered *syn-cis*-orientation of the carbonyl bond (C–O vector) and the C(α)-*H*–C(α) vector of the following residue (minimization of allylic strain [43]). Similary the N–*H* vector and the C(α)–*H*–C(α) vector of the preceding residue prefer the same orien-

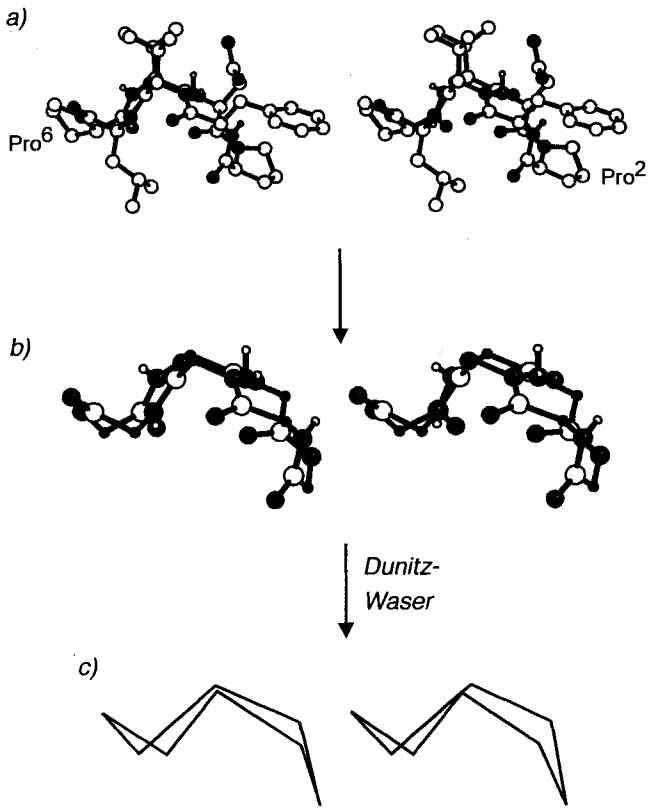

Fig. 8. a) *Side view of axinastatin 2* (**1**) *in DMSO,* b) *connection of the C(α) atoms* (black) *of* **1** *according to the procedure described in the text* (extension of the *Dunitz-Waser* concept to peptides), *and* c) *conformation of* **1** *reduced to the conformation of cyclooctane*

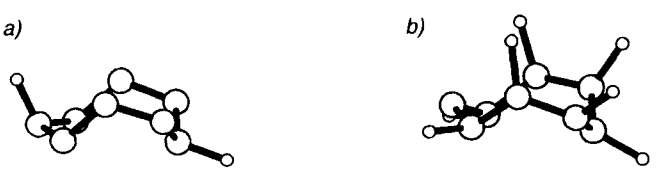

Fig. 9. *Similarity of* a) *the mostly found boat-chair conformation of cyclooctanes such as the X-ray structure of* cis-*cyclooctane-1,5-diol and* b) *the reduced conformation of axinastatin 2* (**1**)

tation. Accordingly for axinastatin 2 (**1**), all CO bonds are in *syn-cis* orientation with the *H*–C(α) protons of the following residue avoiding allylic strain, apart from residue 5 which is involved in the *cis* amide bond.

However, little is known about conformational behavior of higher substituted cyclooctanes. Therefore, it is necessary to keep in mind that a cyclooctane with seven alkyl ('side chain') residues could adopt principally another favored conformation to avoid steric interactions.

3.3. *Biological Results.* Axinastatin 2 (**1**) and 3 (**2**) were tested for inhibition of tumor cell growth in liquid culture of LNCAP lung carcinoma cells, SK-OV-3 ovarian cancer cells, and KB human epidermoid carcinoma cells. Our first results [14] had shown synthetic **1** and **2** to be inactive or of low activity. These results, confirmed by synthetic work by *Pettit* and coworkers in P388 leukaemia cells [44] become now also evident for these cancer cell lines. Up to concentrations of 3.16 μg/ml, no significant inhibition of cancer-cell growth was found for **1** and **2** in any of the used cell lines. To the contrary, a slight stimulation of cancer-cell growth of 18% at 3.16 μg/ml was found for axinastatin 2 (**1**) in the LNCAP cell line.

Axinastatin 4 (**3**) was tested for inhibition of colony formation in soft agar in the KB cell line and additionally in the L1210 leukaemia cell line. However, even at 100 μg/ml, no significant inhibition was found. To check our biological test results, **3** was tested complementary at the NCI in 60 human cancer cell lines (primary antitumor screen [45]). Synthetic **3** was inactive in all cell lines up to 100 μg/ml, except in the ovarian cancer cell line IGROVI, in which a low activity ($GI_{50} = 41$ μg/ml) was found.

In summary, all synthetic compounds, which were identical to the natural products [14], show a significant lower activity than the natural products. These results suggest that natural axinastatin 2 (**1**) and 3 (**2**) might contain undetectable, small amounts of highly active compounds [14] [44]. The strongly antineoplastic polyether macrocyclic lactones halichondrin B and homohalichondrin B, initially isolated from *Halichondria okadai* [3], were also found in *Axinella sp.*, accompanied by axinastatin 1–3 [10] [12]. Natural axinastatin 4 (**3**) from *Axinella cf. carteri* also seems to be accompanied by highly active by-products, such as the sponge halichondrins and halistatins [13].

4. Conclusions. – The conformational analysis of the cyclic heptapeptides axinastatin 2 (**1**), 3 (**2**), and 4 (**3**) by homo- and heteronuclear NMR spectroscopy in combination with DG and MD calculations in explicit solvents is reported. Measurements and calculations in the case of axinastatin 2 (**1**) were performed in DMSO and MeOH. The overall conformations are very similar in both solvents which indicate a rigid backbone conformation. This result differs from stylostatin 1, where different conformational behavior was found depending on the solvent.

Axinastatin 3 (**2**) and 4 (**3**), investigated in DMSO, have backbone conformations very similar to those of **1**. For axinastatin 1 (cyclo(-Asn^1-Pro^2-Phe^3-Val^4-Val^5-Pro^6-Val^7-)), the first member of this family of cyclic heptapeptides [10], a very similar backbone conformation is found too [25]. Axinastatins 1–4 have proline residues in common in position two and six, while the residues at the remaining positions differ. Nevertheless, very similar conformations are found, suggesting that the two proline residues most strongly influence the conformation of these cyclic heptapeptides due to the restricted ϕ angle of proline. Based on comparison of these structures with known conformations of cyclic all-L-peptides, we found the β-bulge motif with two β turns and one bifurcated H-bond as the dominant conformation of cyclic all-L-peptides. Thereby, the *cis*-Pro residue was found to induce mostly the rigid backbone conformation.

The investigated peptides have a boat-chair-like overall backbone conformation which could be rationalized as cyclooctane-like *via* the extension of the *Dunitz-Waser* concept to peptides.

As revealed by the biological tests, the synthetic axinastatins 2–4 (**1**–**3**) show a significant lower activity as initially assumed [12] [13]. Similar results for hymenistatin 1 [46] by our group and stylopeptide [47] by *Pettit* and *Taylor* make a critical reconsideration of these families of cytostatic cyclic peptides necessary. Continuing synthetic work will evaluate the potential biological activity of further cyclopeptides of these families.

Experimental Part

1. *NMR Spectroscopy. General.* All experiments were carried out at 500 MHz for ^{1}H and 125 MHz for ^{13}C on a *Bruker-AMX-500* spectrometer at 300 K. Sample concentration of axinastatin 2 (**1**) was 15 mg in 0.5 ml of (D_6)DMSO (39 mM) and 18 mg in 0.5 ml of CD_3OH (46 mM). Peptide concentration was 15 mg in 0.5 ml of (D_6)DMSO (38 mM) for axinastatin 3 (**2**) and 12 mg in 0.5 ml of (D_6)DMSO (29 mM) for axinastatin 4 (**3**). Temperature coefficients of amide-proton δs were determined between 295 and 320 K in steps of 5°. Intramolecular H/H distances were extracted from ROESY experiments for all compounds. Cross-peak integrals were converted to distance constraints using the isolated two-spin approximation (ISPA) taking the offset correction into account [48]. Due to overlay of Asn^{1}N*H* and Val^{7}N*H* for **1** and **2** in (D_6)DMSO at 300 K, H distances from these H were obtained from additional ROESY experiments at 294 K, where the N*H* δs of Asn^1 and Val^7 were resolved. By comparing the remaining H/H distances, no differences and hence no conformational changes between 300 and 294 K were observed. ^3J(N*H*,*H*–C(α)) coupling constants of Asn^1 and Val^7 were also determined at 294 K. ROESY and 1D ^{1}H-NMR experiments at 294 and 300 K were realized with analogous parameters.

Investigations in (D_6)DMSO. All homonuclear experiments were recorded with a spectral width of 5000 Hz (**1** and **2**) and 6666 Hz (**3**) in both dimensions. HMQC and HMQC-COSY experiments were recorded with a spectral width of 12194 Hz in t_1 and HMBC experiments with a spectral width of 13834 Hz in t_1. TOCSY Experiments were recorded with a MLEV-17 mixing sequence of 80 ms duration, 10 kHz spin-lock field, 64 scans, 2048 data points in t_2 and 512 points in t_1. P.E.COSY experiments were recorded with 8192 data points in t_2, 512 in t_1, and 32 scans. The reference 1D ^{1}H-NMR was recorded with 16384 data points, and the relaxation delay was set equal to the relaxation delay of the 2D experiment reduced by the acquisition time of the 2D experiment. Compensated 2D-ROESY experiments with pulsed spin-lock field [49] (3 kHz) were recorded with 4096 data points in t_2, 512 data points in t_1, τ_{mix} 200 ms, and 48 scans. HMQC and HMQC-COSY experiments were recorded with 2048 data points in t_2, 512 data points in t_1, and 64 scans. For suppression of protons bound to ^{12}C, a BIRD pulse [50] was used with an optimized delay of 160 ms. HMBC Experiments were recorded with low pass *J*-filter [51] with 4096 data points in t_2, 384 data points in t_1, and 128 scans. 1D ^{1}H and ^{13}C-NMR experiments were recorded with standard parameters.

Investigations in CD_3OH. Experiments and spectral parameters were similar to those for (D_6)DMSO solns. Additionally, for all experiments (except HMQC), presaturation of 1s during the relaxation delay was set on the ^{1}H frequency of CD_3OH to suppress the resonance of the solvent. The P.E.COSY experiment was replaced by an E.COSY experiment with presaturation, recorded with 8192 data points in t_2, 512 in t_1, and 36 scans. Chemical shifts δ(H) are reported in ppm rel. to residual (D_5)DMSO (δ 2.49) or CD_2HOH (δ 3.30), and δ(C) rel. to (D_6)DMSO (δ 39.5) and CD_3OH (δ 49.0).

2. *Computer Simulations.* The preliminary structure was generated by a modified version [52] of the DISGEO [53] program. For axinastatin 2 (**1**) in MeOH, 63 distance restraints, for **1** in DMSO, 60 distance restraints, for axinastatin 3 (**2**) in DMSO, 64 distance restraints, and for axinastatin 4 (**3**) in DMSO, 58 distance restraints were introduced. Introduction of 11 dihedral angles for each calculation was performed by using the full *Karplus* curve [54]. Thus, 100 structures were embedded and refined by distance-driven dynamics [55] and by distance- and angle-driven dynamics [56] in the four- and three-dimensional space. The low-error structure was refined by 150 ps of restraint molecular dynamics in explicit DMSO [57] or MeOH [58] using the DISCOVER [59] program with the CVFF [60] force field. For **1** and **3** a fMD calculation of 90 ps was performed. After 10 ps for equilibration, within 30 ps, the distance restraints were scaled down. All MD calculations were performed at 300 K in a cubic box of 33 Å. A cutoff of 12 Å was used. Distances from the simulations were calculated by $< r^{-3} >^{-1/3}$ [61].

3. *Biological Testing.* Biological tests have been described previously [46] [45].

Financial support by the *Deutsche Forschungsgemeinschaft* (*SFB 369*) and the *Fonds der Chemischen Industrie* is gratefully acknowledged. We thank *NCI* (*National Cancer Institute*) for *in-vitro* testing of synthetic axinastatin 4 (**3**) in the primary antitumor screen. We appreciate helpful discussion of Dr. *J. Schmidt* and Dr. *R. Voegeli*, *ASTA Medica*.

REFERENCES

[1] G. M. König, A. D. Wright, *Planta Med.* **1996**, *62*, 193.
[2] G. R. Pettit, Y. Kamao, C. L. Herald, A. A. Tuinman, F. E. Boettner, H. Kizu, J. M. Schmidt, L. Baczynskyj, K. B. Tomer, R. J. Bontems, *J. Am. Chem. Soc.* **1987**, *109*, 6883.
[3] Y. Hirata, D. Uemura, *Pure Appl. Chem.* **1986**, *58*, 701.
[4] K. L. Rinehart, Jr., J. B. Gloer, R. G. Hughes, Jr., H. E. Renis, J. P. McGovren, E. B. Swynenberg, D. A. Stringfellow, S. L. Kuentzel, L. H. Li, *Science* **1981**, *212*, 933.
[5] G. R. Pettit, C. L. Herald, D. L. Doubek, D. L. Herald, *J. Am. Chem. Soc.* **1982**, *104*, 6846.
[6] F. Flam, *Science* **1994**, *266*, 1324.
[7] G. R. Pettit, J. K. Srirangam, D. L. Herald, J.-P. Xu, M. R. Boyd, Z. Cichacz, Y. Kamano, J. M. Schmidt, K. L. Erickson, *J. Org. Chem.* **1995**, *60*, 8257.
[8] G. R. Pettit, J. K. Srirangam, D. L. Herald, K. L. Erickson, D. L. Doubek, J. M. Schmidt, L. P. Tacket, G. J. Bakus, *J. Org. Chem.* **1992**, *57*, 7217.
[9] G. R. Pettit, P. J. Clewlow, C. Dufresne, D. L. Doubek, *Can. J. Chem.* **1990**, *68*, 708.
[10] G. R. Pettit, C. L. Herald, M. R. Boyd, J. E. Leet, C. Dufresne, D. L. Doubek, J. M. Schmidt, R. L. Cerny, J. N. A. Hooper, K. C. Rützler, *J. Med. Chem.* **1991**, *34*, 3339.
[11] H. Kessler, *Angew. Chem. Int. Ed.* **1982**, *21*, 512.
[12] G. R. Pettit, F. Gao, R. L. Cerny, D. L. Doubek, L. P. Tackett, J. M. Schmidt, J.-C. Chapuis, *J. Med. Chem.* **1994**, *37*, 1165.
[13] G. R. Pettit, F. Gao, R. Cerny, *Heterocycles* **1993**, *35*, 711.
[14] O. Mechnich, H. Kessler, *Tetrahedron Lett.* **1996**, *37*, 5355.
[15] D. S. Eggleston, P. W. Baures, C. E. Peishoff, K. D. Kopple, *J. Am. Chem. Soc.* **1991**, *113*, 4410.
[16] H. Morita, T. Kayashita, K. Takeya, H. Itokawa, M. Shiro, *Tetrahedron* **1995**, *51*, 12539.
[17] H. Kessler, M. Bernd, *Liebigs Ann. Chem.* **1985**, 1145.
[18] C. Griesinger, H. Schwalbe, J. Schleucher, M. Sattler, in 'Two-Dimensional NMR Spectroscopy', Eds. W. R. Croasmun and R. M. K. Carlson, VCH, Weinheim, 1994, pp. 458–580.
[19] H. Kessler, S. Seip, in 'Two-Dimensional NMR Spectroscopy', Eds. W. R. Croasmun and R. M. K. Carlson, VCH, Weinheim, 1994, pp. 619–654; H. Kessler, W. Schmitt, in 'Encyclopedia of Nuclear Magnetic Resonance', Eds. D. M. Grandt and R. K. Harris, John Wiley & Sons, Chichester, 1996, Vol. 6, p. 3527.
[20] M. Eberstadt, G. Gemmecker, D. F. Mierke, H. Kessler, *Angew. Chem. Int. Ed.* **1995**, *34*, 1671.
[21] D. E. Dorman, F. A. Borvey, *J. Org. Chem.* **1973**, *38*, 1719.
[22] D. E. Dorman, F. A. Borvey, *J. Org. Chem.* **1973**, *38*, 2379.
[23] A. Abbadi, M. Mcharfi, A. Aubry, S. Premilat, G. Boussard, M. Marraud, *J. Am. Chem. Soc.* **1991**, *113*, 2729.
[24] K. G. R. Pachler, *Spectrochim. Acta* **1963**, *19*, 2085.
[25] R. K. Konat, B. Mathä, J. Winkler, H. Kessler, *Liebigs Ann. Chem.* **1995**, 765.
[26] H. Kessler, A. Friedrich, *J. Org. Chem.* **1981**, *46*, 3892.
[27] G. R. Pettit, J. K. Srirangan, D. L. Herald, K. L. Erickson, D. L. Doubek, J. M. Schmidt, L. P. Tackett, G. J. Bakus, *J. Org. Chem.* **1992**, *57*, 7217.
[28] H. Kessler, E. Planker, R. Gschwind, R. K. Konat, unpublished results.
[29] H. Matter, G. Gemmecker, H. Kessler, *Int. J. Pept. Protein Res.* **1995**, *45*, 430.
[30] H. Kessler, J. W. Bats, C. Griesinger, S. Koll, M. Will, K. Wagner, *J. Am. Chem. Soc.* **1988**, *110*, 1033; M. Gerz, H. Matter, H. Kessler, *Int. J. Pept. Protein Res.* **1994**, *43*, 248.
[31] P. Groth, *Acta Chem. Scand., Sect. A* **1975**, *29*, 38.
[32] G. R. Pettit, Z. Cichacz, J. Barkoczy, A.-C. Dorsaz, D. L. Herald, M. D. Williams, D. L. Doubek, J. M. Schmidt, L. P. Tackett, D. C. Brune, *J. Nat. Prod.* **1993**, *56*, 260.
[33] H. Morita, T. Kayashita, K. Takeya, H. Itokawa, M. Shiro, *Tetrahedron* **1997**, *53*, 1607.
[34] C. E. Peishoff, J. W. Bean, K. D. Kopple, *J. Am. Chem. Soc.* **1991**, *113*, 4416.
[35] J. Kobayashi, M. Tsuda, T. Nakamura, Y. Mikami, H. Shigemori, *Tetrahedron* **1993**, *49*, 2391; M. Tsuda, H. Shigemori, Y. Mikami, J. Kobayashi, *ibid.* **1993**, *49*, 6785; J. Kobayashi, T. Nakamura, M. Tsuda, *ibid.* **1996**, *52*, 6355.
[36] G. R. Pettit, R. Tan, D. L. Herald, R. L. Cerny, W. D. Williams, *J. Org. Chem.* **1994**, *59*, 1593.
[37] J. S. Richardson, E. D. Getzoff, D. C. Richardson, *Proc. Natl. Acad. Sci. U.S.A.* **1978**, *75*, 2574.
[38] G. Müller, M. Gurrath, M. Kurz, H. Kessler, *Proteins: Struct., Funct. Genet.* **1993**, *15*, 235.
[39] H. Kessler, R. Gratias, G. Hessler, M. Gurrath, G. Müller, *Pure Appl. Chem.* **1996**, *68*, 1201.

[40] J. D. Dunitz, J. Waser, *J. Am. Chem. Soc.* **1972**, *94*, 5645.
[41] F. A. L. Anet, *Fortschr. Chem. Forsch.* **1974**, *45*, 169.
[42] R. W. Miller, A. T. McPhail, *J. Chem. Soc., Perkin Trans. 2* **1979**, 1527.
[43] R. W. Hoffmann, *Angew. Chem. Int. Ed.* **1992**, *31*, 1124.
[44] G. R. Pettit, J. W. Holman, G. M. Boland, *J. Chem. Soc., Perkin Trans. 1* **1996**, 2411.
[45] M. R. Boyd, *Principles Pract. Oncol.* **1989**, *10*, 1.
[46] R. K. Konat, D. F. Mierke, H. Kessler, B. Kutscher, M. Bernd, R. Voegeli, *Helv. Chim. Acta* **1993**, *76*, 1649.
[47] G. R. Pettit, S. R. Taylor, *J. Org. Chem.* **1996**, *61*, 2322.
[48] C. Griesinger, R. R. Ernst, *J. Magn. Reson.* **1987**, *75*, 261.
[49] H. Kessler, C. Griesinger, R. Kerssebaum, K. Wagner, R. R. Ernst, *J. Am. Chem. Soc.* **1987**, *109*, 607.
[50] J. R. Garbow, D. P. Weitekamp, A. Pines, *Chem. Phys. Lett.* **1982**, *93*, 504.
[51] H. Kogler, O. W. Sørensen, G. Bodenhausen, R. R. Ernst, *J. Magn. Reson.* **1983**, *55*, 157.
[52] D. F. Mierke, H. Kessler, *Biopolymers* **1993**, *33*, 1003.
[53] T. F. Havel, *Prog. Biophys. Mol. Biol.* **1991**, *56*, 43; G. M. Crippen, T. F. Havel, 'Distance Geometry and Molecular Conformation', Research Studies Press LTD., Somerset, England, John Wiley & Sons, New York, 1988; T. F. Havel, 'DISGEO, Quantum Chemistry Exchange Program, Exchange No. 507', Indiana University, 1986; T. F. Havel, K. Wüthrich, *Bull. Math. Bio.* **1984**, *46*, 673.
[54] D. F. Mierke, T. Huber, H. Kessler, *J. Comput. Aided Mol. Des.* **1994**, *8*, 29.
[55] R. M. Scheek, A. E. Torda, J. Kenmink, W. F. van Gunsteren, in 'Computational Aspects of the Study of Biological Macromolecules by Nuclear Magnetic Resonance', Plenum Press, New York, 1991, p. 209; J. Kenmink, C. P. M. van Mierlo, R. M. Scheek, T. E. Creighton, *J. Mol. Biol.* **1993**, *230*, 312.
[56] D. F. Mierke, R. M. Scheek, H. Kessler, *Biopolymers* **1994**, *34*, 559.
[57] D. F. Mierke, H. Kessler, *J. Am. Chem. Soc.* **1991**, *113*, 9466.
[58] W. L. Jorgensen, *J. Phys. Chem.* **1986**, *90*, 1276; W. L. Jorgensen, *J. Am. Chem. Soc.* **1980**, *102*, 543.
[59] 'DISCOVER Version 2.97', BIOSYM Technologies, 10065 Barnes Canyon Road, San Diego, CA 92121, USA.
[60] A. T. Hagler, S. Lifson, P. Dauber, *J. Am. Chem. Soc.* **1979**, *101*, 5122.
[61] H. Kessler, C. Griesinger, J. Lautz, A. Müller, W. F. van Gunsteren, H. J. C. Berendsen, *J. Am. Chem. Soc.* **1988**, *110*, 3393.